



## Enhancement of Polystyrene Nanocomposites with THDACI-Modified Montmorillonite via Melt Compounding

Saiga Amira<sup>1\*</sup>, Zidelkheir Belkacem<sup>1</sup>, Smail Terchi<sup>2</sup>, Ghania Benaiche<sup>3</sup>

<sup>1</sup> Research Laboratory Cities, Environment, Society and Sustainable Development (CESSD), Department of Chemistry, Faculty of Sciences, University Mohamed BOUDIaf -M'Sila, M'Sila 28000, Algeria

<sup>2</sup> Department of Chemistry, Faculty of Sciences, University Mohamed BOUDIaf -M'Sila, M'Sila 28000, Algeria

<sup>3</sup> Department of Microbiology and Biochemistry, Faculty of Sciences, University Mohamed BOUDIaf -M'Sila, M'Sila 28000, Algeria

Corresponding Author Email: [amira.saigaa@univ-msila.dz](mailto:amira.saigaa@univ-msila.dz)

Copyright: ©2024 The authors. This article is published by IETA and is licensed under the CC BY 4.0 license (<http://creativecommons.org/licenses/by/4.0/>).

<https://doi.org/10.18280/acsm.480211>

### ABSTRACT

**Received:** 6 November 2023

**Revised:** 22 January 2024

**Accepted:** 10 April 2024

**Available online:** 30 April 2024

#### Keywords:

*PS nanocomposites, clay modification, surfactant intercalation, THDACI-MMT, interlayer distance, d-spacing, dispersion enhancement, mechanical properties, thermal stability, TEM*

The research findings on PS nanocomposites prepared with N,N,N-trimethyl-1-hexadecyl ammonium chloride (THDACI) reveal improved dispersion, enhanced mechanical properties, and increased thermal stability. These advancements have significant implications for various industries, including automotive, aerospace, packaging, and electronics, where the nanocomposites can be utilized for lightweight structural components, flame-resistant coatings, and high-performance packaging materials. Increasing the interlayer distance (d-spacing) of fractionated sodium montmorillonite (FMMT-Na) using N,N,N-trimethyl-1-hexadecyl ammonium chloride (THDACI) is done to improve the compatibility and dispersion of the clay in polymer matrices. This modification is relevant and beneficial as it enhances the mechanical properties, barrier performance, and thermal stability of the resulting nanocomposites, opening up opportunities for various applications in industries such as packaging, automotive, construction, and electronics. PS nanocomposites were prepared by incorporating MMT clay using THDACI as a surfactant. The composition ratios included 1-10% weight percentage of MMT with a 1:1 weight ratio of THDACI to MMT. The melt compounding process involved treating MMT with THDACI, dispersing it in a solvent, and adding it to melted PS pellets. Characterization techniques, such as XRD, TEM, SEM, TGA, and mechanical testing, were used to evaluate the nanocomposites. The results demonstrated improved dispersion, enhanced mechanical properties, and increased thermal stability. These findings contribute to the optimization of the nanocomposites for specific applications.

## 1. INTRODUCTION

The use of sodium montmorillonite (Na-MMT) as a nanofiller in polymer clay nanocomposites has gained considerable attention due to its potential to enhance the mechanical properties, heat resistance, and barrier properties of the resulting materials. Several studies have reported significant improvements in these properties when incorporating Na-MMT into polymer matrices.

Jiang et al. [1] investigated the mechanical properties of polypropylene (PP)/montmorillonite nanocomposites by intercalating compatibilizers into the clay layers. They observed a substantial increase in tensile strength and modulus compared to pure PP. Similarly, Ray and Okamoto [2] provided a comprehensive review highlighting the improved mechanical properties, including increased stiffness and strength, in various polymer/layered silicate nanocomposites.

Studies have also demonstrated the enhanced heat resistance of Na-MMT nanocomposites. Liu et al. [3] investigated the thermal stability and degradation kinetics of

polypropylene/montmorillonite nanocomposites. They found that the presence of Na-MMT led to improved thermal stability and higher degradation temperatures compared to pure polypropylene. Additionally, Zhang et al. [4] studied the thermal stability and flammability of polypropylene/montmorillonite nanocomposites and reported increased thermal stability and reduced flammability due to the incorporation of Na-MMT.

The barrier properties of polymer nanocomposites can be significantly enhanced by incorporating Na-MMT. Li et al. [5] evaluated the barrier performance of poly (lactic acid) nanocomposite films with different nanoclays and found that the addition of Na-MMT led to improved gas barrier properties. Rhim and Ng [6] investigated the effect of clay content on the physical and mechanical properties of nanocomposite films based on poly (lactic acid) and reported enhanced oxygen and water vapor barrier properties with the addition of Na-MMT.

These examples demonstrate the positive impact of incorporating Na-MMT into polymer nanocomposites, leading to improved mechanical properties, heat resistance, and barrier

properties. By providing specific references and examples, the credibility of the claims is enhanced, and readers gain a better understanding of the significance of the research.

The use of polymer/clay nanocomposites has attracted significant research interest due to their potential for improving material properties. However, there is a research gap in the synthesis of polystyrene (PS)/clay nanocomposites using nanoclays modified with various organo-modifiers. To the best of our knowledge, no studies have explored the synthesis and characterization of PS/clay nanocomposites using this approach. This research gap presents an opportunity to investigate the effects of different organo-modifiers on the properties of PS-based nanocomposites.

The novelty of this study lies in the investigation of PS/clay nanocomposites using nanoclays modified with various organo-modifiers. By systematically studying the effects of different organo-modifiers on the dispersion, mechanical properties, thermal stability, and other relevant characteristics of the nanocomposites, we aim to fill the existing research gap and provide a comprehensive understanding of the impact of organo-modifiers on the properties of PS-based nanocomposites. The outcomes of this research will contribute to the design and development of advanced polymer nanocomposites with tailored properties for various applications.

## 2. METHODOLOGY

### 2.1 Materials

Natural clays from the Magnia Zone (Algeria) were used in the experiments. The surfactant N,N,N-trimethyl-1-hexadecyl ammonium chloride (THDACI) was purchased from SIGMA-ALDRICH, Germany.

#### 2.1.1 Montmorillonite sodium synthesis

To start with, magnesia dirt was blended in deionized water and 30% hydrogen peroxide (H<sub>2</sub>O<sub>2</sub>) for 48 hours to eliminate natural matter. The following stage comprised of adding the magnesia montmorillonite (MMT) answer for a NaCl arrangement containing CEC (95 meq/100 g), which was blended at (60°C) for 5 hours. The subsequent suspension was then washed a few times with refined water utilizing centrifugation to eliminate all chloride particles (utilizing 0.1 N trial of silver nitrate (AgNO<sub>3</sub>) arrangement).

The precipitate was then dried in a vacuum broiler at 80°C for 24 hours. The item was ground and sieved at 90 µm for different purposes. The montmorillonite suspension was set in a rotator tube and suctioned with a needle to gather the montmorillonite portion with a molecule size of 2 µm. The waste was then gathered and supplied for additional utilization. The subsequent example was centrifuged at 4000 rpm for 20 minutes. The gathered suspension was dried at 80°C and ground in a mortar. The fractionated sodium montmorillonite was assigned FMMT-Na.

#### 2.1.2 Organo-montmorillonite synthesis (THDACI-MMT)

The synthesis of organo-montmorillonite was performed using the following procedure: 3.52 g of fractionated sodium montmorillonite were dispersed in 100 ml of hot deionized water (60°C) gradually then magnetic stirred for 1h. 1 g of THDACI, was dissolved in a mixture of deionized water and hydrochloric acid (36%) at 60°C during 2 h with stirring.

The mixture was let themselves at ambient temperature without stirring for approximately 24 h. After reaction, the white precipitate was isolated by filtration and the excess of chloride and organic ions was removed by repeated washing with deionized water at 80°C until a negative result of the AgNO<sub>3</sub> test was obtained. The precipitate was then dried to obtain organomontmorillonite with N, N, N- trimethyl-1-hexadecylammonium chloride (THDACI-MMT).

#### 2.1.3 Nanocomposites synthesis PS/THDACI-MMT

A mixture of 57.2 g of polystyrene (PS) and THDACI-MMT was melt-kneaded at 240°C (Ps) and high rotor speed (60 rpm) for 30 min at Brabender GmbH & Co. KG at 1%, 3% and 7% loading as shown in Table 1.

**Table 1.** The compositions of the systems

Systems	PS (g)	THDACI-MMT (g)	Time (min)
PS/THDACI-MMT 1%	56.62	0.57	30
PS/THDACI-MMT 3%	55.42	1.72	30
PS/THDACI-MMT 7%	53.20	4.00	30

### 2.2 Characterization instruments

X-ray diffraction (XRD) patterns were obtained using a spinner PW 3064 (Cu Ka radiation,  $k = 1.5418 \text{ \AA}$ ) at 45 kV, 30 mA, and a scanning speed of 0.01°/min to obtain X-ray diffraction patterns. The  $d_{001}$  spacing of the clay was calculated using Bragg's law.

$$d(hkl) = \lambda/2 \sin \theta \max$$

FT-IR measurements were performed on a Shimadzu 8300 Fourier-transform IR spectrometer.

Thermogravimetric (TG) and DTA analyses were performed under a nitrogen atmosphere using a DW5470H63 STA analyzer. The temperature was increased from room temperature to 950°C at a rate of 10°C/min<sup>-1</sup>.

Clay samples were prepared for elemental chemical analysis using the so-called fusion bead method.

A Rigaku ZSX Primus IV was used for analysis of transparent beads. A scanning electron microscope (SEM) PHILIPS ESEM XL 30 with a tungsten fiber was utilized to concentrate on the morphology of the concentrated-on examples with conductive carbon paint.

TEM is an instrument created to comprehend the interior microstructure of materials, particularly earth minerals, at the sub-nanometer level. The examination was recorded on a Phillips CM 20 instrument and the speed increase voltage of the microscope lens was 120 kV.

## 3. SECTION HEADINGS

### 3.1 XRF results

THDACI-MMT analysis has been performed after obtaining the biggest basal spacing of the silicate layers. Authors [7] highlight that XRF quantitative analysis of pure and sodium montmorillonite shows a rise in the percentage of

Na<sub>2</sub>O ions from 0.01 to 2.66, confirming the intercalation of sodium ions in the interfoliar space. The decrease in the content of CaO and MgO at cation exchangeable cations of sodium. The decrease in oxide levels (Fe<sub>2</sub>O<sub>3</sub>, TiO<sub>2</sub>, and ZrO<sub>2</sub>) is due to the cationic replacement that ensures the saturation of sodium clay. The results in Table 2 show that the percentage of Na<sub>2</sub>O decreased.

**Table 2.** Summary of the chemical composition of MMT, MMT-Na and THDACI-MMT obtained from XRF-analysis

Compositions (%)	MMT	FMMT-NA	THDACI-MMT
Na <sub>2</sub> O	0.01	2.66	0.47
CuO	-	-	-
MgO	3.37	3.30	3.33
Al <sub>2</sub> O <sub>3</sub>	24.15	17.72	21.3
SiO <sub>2</sub>	67.6	72.7	67.0
P <sub>2</sub> O <sub>5</sub>	0.013	0.01	0.019
CaO	0.01	0.01	0.13
MnO	0.17	0.175	0.045
Fe <sub>2</sub> O <sub>3</sub>	0.09	-	0.09
ZnO	2.80	1.95	0.01
TiO <sub>2</sub>	0.013	0.011	0.27
ZrO <sub>2</sub>	0.013	0.010	0.014

### 3.2 XRD results

The diffraction diagram of crude MMT-montmorillonite is shown in Figure 1. Fractionated sodium montmorillonite FMMT-Na and organic solvent THDACI-MMT. DRX spectra of raw MMT and FMMT-Na show the same peak corresponding to (001) Wang et al. [8] announced the following values ( $2\theta = 5.78$ ,  $d_{001} = 15.19 \text{ \AA}$ ).

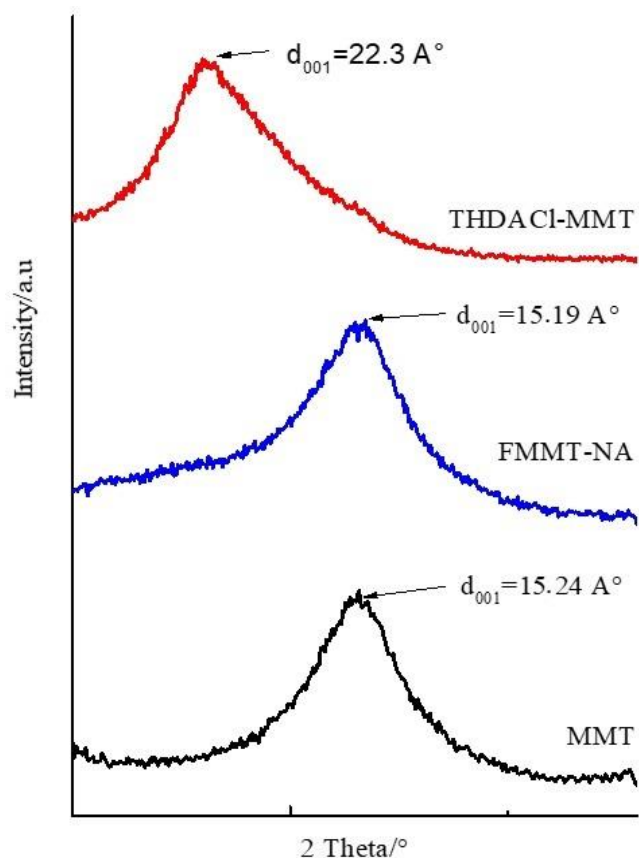


**Figure 1.** XRD diagrams of virgin (MMT), fractionated (FMMT-Na), and organo-montmorillonite modified by alkyl ammonium (THDACI-MMT)

Intercalation of clays by THDACI increases the interphoreal space ( $2\theta = 4^\circ$ ) corresponding to  $d_{001} = 22.3 \text{ \AA}$ , which is twice the van der Waals diameter of the trimethyl group [9, 10], as the alkylamine (ammonium) carbon chain increases, the interlayer clay interfacial space increases [11].

A large peak appears in the  $2\theta \sim 5.7^\circ$  direction, which may be due to the large-scale organization of the silicate [2].

DRX spectra of nanocomposite PS/OMMT (THDACI-MMT) with various OMMT loadings are shown in Figure 2 (1%, 3%, 7%).

Diffraction peaks corresponding to large spaces at  $2\theta$  ( $2.03^\circ$ ,  $2.04^\circ$ , and  $2.08^\circ$ ) were detected for PS/THDACI-MMT 1%, 3%, and 7%.

The presence of intercalated structures was suggested by interholds at  $43.4 \text{ \AA}$  for PS/THDACI-MMT 1%,  $43.2 \text{ \AA}$  for PS/THDACI-MMT 3%, and  $42.4 \text{ \AA}$  for 7%, confirming intercalated nanocomposite structures. The increased d-spacing confirmed that the polymer chains intercalated between the clay layers [12].

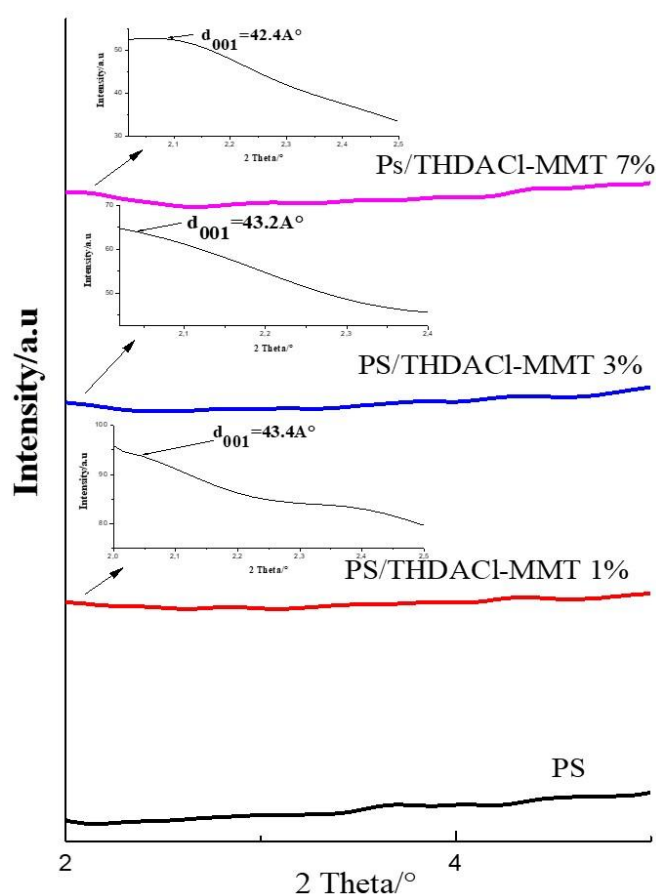


**Figure 2.** XRD diagrams of THDACI-MMT and PS/THDACI-MMT (1%, 3%, and 7%)

### 3.3 FTIR results

Intercalation of organic salts into clay mineral interlayers is often evaluated using infrared spectroscopy [13-23].

In Figure 3, the band at  $3633 \text{ cm}^{-1}$  is associated with antisymmetric stretching vibrations of structural -OH groups, symmetric stretching vibrations from water appear clearly around  $3447 \text{ cm}^{-1}$ , and an absorption band located at  $1641 \text{ cm}^{-1}$  is attributed to angular deformation of the inter-polar water and is attributed to observed structural changes in montmorillonite with important sensitivity and positive

response [14]. As for the deformation bands of metals bonded to hydroxyl groups, several band adsorption frequencies characteristic of metallic elements appear at the frequencies of Al-OH-Al:  $909\text{ cm}^{-1}$  and Mg-Al-OH:  $844\text{ cm}^{-1}$  [15]. The band at  $1023\text{--}1136\text{ cm}^{-1}$  corresponds to the elongation vibration of SiO; the  $511\text{ cm}^{-1}$  band corresponds to deformation vibrations of SiO bonds; small amounts of impurities are present at  $698\text{ cm}^{-1}$  (quartz) and  $795\text{ cm}^{-1}$  (tridymite) [16]. For organophilic THDACI-MMT, the interaction of FMMT-Na with the surface-active cation THDACI-MMT results in the showing of new bands at  $2928\text{ cm}^{-1}$  and  $2855\text{ cm}^{-1}$  due to antisymmetric and symmetric elongation vibrations of the  $\text{CH}_2$  groups in the alkyl chains. The bands corresponding to the valence vibrations of the OH groups of the water molecule are found to be reduced compared to FMMT-Na. This observation confirms the new hydrophobic nature of montmorillonite.

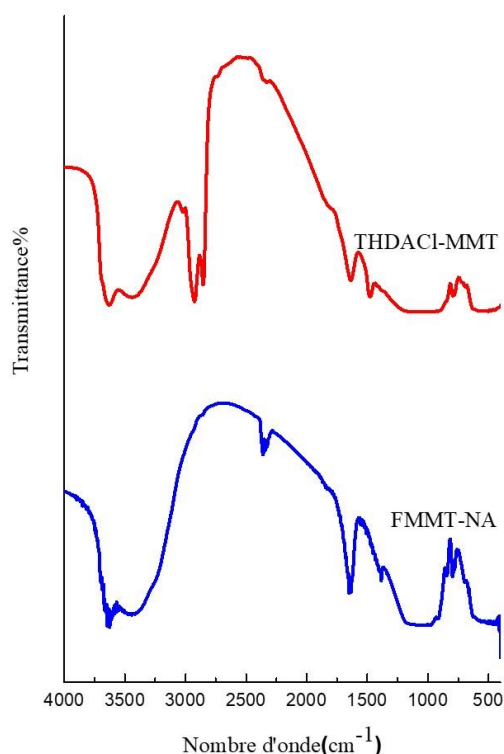


**Figure 3.** FTIR spectra of FMMT-Na and (THDACI-MMT)

As for the deformation bands of metals bonded to hydroxyl groups, some adsorption frequencies characteristic of metallic elements appears at the frequencies of Al-OH-Al:  $909\text{ cm}^{-1}$ , Mg-Al-OH:  $844\text{ cm}^{-1}$  [15]. The band at  $1023\text{--}1136\text{ cm}^{-1}$  corresponds to SiO elongation vibrations; at  $511\text{ cm}^{-1}$  band corresponds to deformation vibrations of SiO bonds; small amounts of impurities are present at  $698\text{ cm}^{-1}$  (quartz) and  $795\text{ cm}^{-1}$  (tridymite) [16]. For organophilic THDACI-MMT, the interaction of FMMT-Na with the surface-active cation THDACI-MMT results in the showing of new bands at  $2928\text{ cm}^{-1}$  and  $2855\text{ cm}^{-1}$  due to antisymmetric and symmetric elongation vibrations of the  $\text{CH}_2$  groups in the alkyl chains. The bands corresponding to the valence vibrations of the OH groups of the water molecule are found to be reduced compared to FMMT-Na. This observation confirms the new hydrophobic nature of montmorillonite.

FTIR spectroscopy confirmed the insertion of surfactant molecules. In fact, new absorption bands attributed to the surfactant molecules used appear in the montmorillonite sheets, indicating a decrease in the amount of water. This suggests a

chemical modification of montmorillonite to change its hydrophilic and organophobic nature to organophilic and hydrophobic [17].

In Figure 4, both polymeric organic and inorganic groups are prominent in the PS/THDACI-MMT spectra (1%, 3%, and 7%): at  $3220\text{ cm}^{-1}$  (PS/THDACI-MMT 1%),  $3744\text{ cm}^{-1}$  (PS/THDACI-MMT 3%), and  $2930\text{ cm}^{-1}$  (PS/THDACI-MMT 7%). The aromatic C-H and aliphatic stretching vibrations cause characteristic peaks around  $3027\text{ cm}^{-1}$  and  $2926\text{ cm}^{-1}$  in the PS spectrum, respectively. The spectra reveal bands of C=C stretching vibrations at  $1595$ ,  $1494$ , and  $1449\text{ cm}^{-1}$ , a  $\text{CH}_2$ -based vibrational mode at  $1371\text{ cm}^{-1}$ , and a C-H benzene stretching vibration at  $699\text{ cm}^{-1}$ .

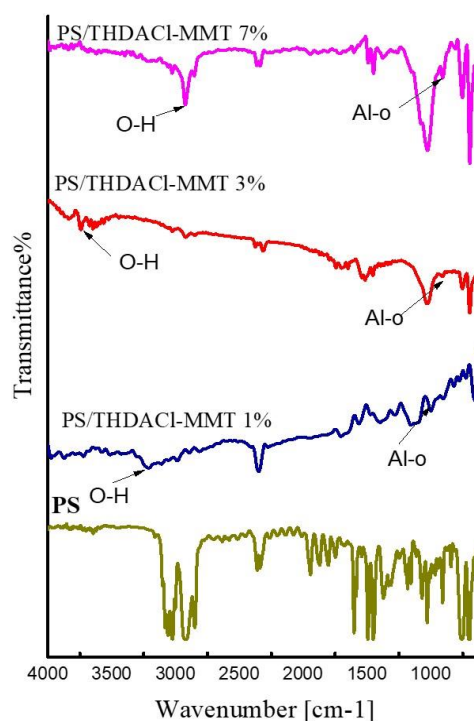


**Figure 4.** FTIR spectra of THDACI-MMT and PS/THDACI-MMT (1%, 3%, and 7%)

As shown in Figure 4, in PS/THDACI-MMT, organic and inorganic macromolecular groups are clearly visible in the spectra (1%, 3%, and 7%). Furthermore, the new bands at  $3220\text{ cm}^{-1}$  (PS/THDACI-MMT 1%),  $3744\text{ cm}^{-1}$  (PS/THDACI-MMT 3%), and  $2930\text{ cm}^{-1}$  (PS/THDACI-MMT 7%) are attributed to the O-H stretching of the structural hydroxyl groups, while at  $1002\text{ cm}^{-1}$  (PS/THDACI-MMT 1%), Al-O stretching at  $945\text{ cm}^{-1}$  (PS/THDACI-MMT 1%) and  $912\text{ cm}^{-1}$  (PS/THDACI-MMT 1%), and Si-O stretching at  $1157\text{ cm}^{-1}$ ,  $1024\text{ cm}^{-1}$  and  $1012\text{ cm}^{-1}$  in the tetrahedral silica layer of modified clay [18].

According to all these confirmations, the organic affinity layer is chemically bonded to PS to produce PS/THDACI-MMT nanocomposites.

### 3.4 TG -DSC results

The thermogravimetric (TG) and subordinate (DTG) changes of FMMT-Na under idle environment are displayed in Figure 5. These outcomes, got at  $52^\circ\text{C}$  and  $520^\circ\text{C}$ , connect with the accompanying mass misfortunes: the principal mass misfortune (11%) somewhere in the range of  $30^\circ\text{C}$  and  $170^\circ\text{C}$  is because of the vaporization of free water in this

montmorillonite and the drying out of Na<sup>+</sup> cations in interlayer spaces [17], certain pores and exhibitions. The second mass misfortune (3%) somewhere in the range of 488°C and 678°C is because of the arrival of water related with the recombination of hydroxyl bunches on the sheet surface. On account of organophilic dirt, the warm peculiarities recorded are as per the following: mass misfortune at around 200°C (mass misfortune 4%), connected with the vaporization of free water contained in this montmorillonite and alluding to the trading of hydrated Na<sup>+</sup> cations with surfactant cations [19]. The disintegration temperature of surfactants goes from 200°C to 500°C. Notwithstanding, dehydrogenation of aluminosilicates happens somewhere in the range of 490°C and 650°C. Burning responses of inorganic materials containing natural carbon and oxygen (wood carbon ignition) are related with a last stage above 700°C.

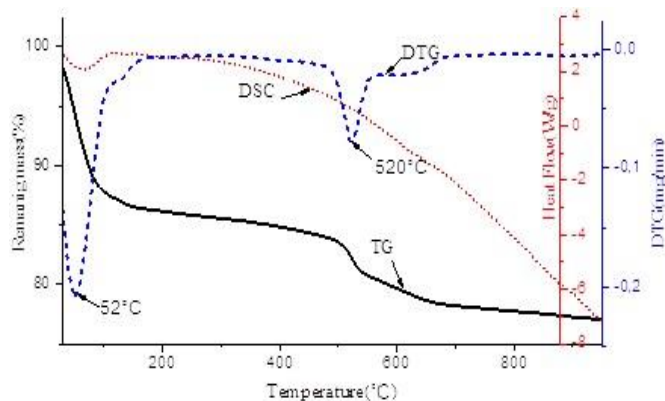


**Figure 5.** TG, DTG, and DSC bends of fractionated montmorillonite

On the other hand, the natural dissolvable THDACI-MMT (Figure 6) displayed three unmistakable sub-atomic conditions for surfactants in montmorillonite-ammonium organoclay:

- surfactant cations are intercalated into the interlayer space by cation trade and tie to surface locales by electrostatic associations.
- surfactant (cations and additionally atoms) genuinely adsorbed on the external surface of the molecule.
- surfactant atoms present in the interlayer space.

In their review [20], they show that surfactant particles over the CEC stick to the dirt mineral surface by averaging van der Waals powers. Moreover, these particles show properties basically the same as those of unadulterated surfactants. Surfactants genuinely adsorbed on the outer surface might be eliminated subsequent to washing, prompting an expansion in warm soundness and a diminishing in the surface energy of the subsequent organoclay [21]. The DSC bends of FMMT-Na and the natural compound THDACI-MMT are displayed in Figure 5. It shows that one critical endothermic change happened at 63°C. The last option is connected with the volatilization of water and free water present in the interlayer space framing hydration circles around the replaceable cations;

the temperature around 70°C is because of the parchedness of montmorillonite. What's more, an exothermic response was seen around 339.8°C (THDACI-MMT). This change is because of the decay and oxidation of free surfactants as well as those adsorbed on the external surface of montmorillonite. One more change is seen around 451.2°C (THDACI-MMT) and is because of the ceaseless corruption of adsorbed and intercalated alkylammonium cations. These cations are related with the most extreme pace of thermo-oxidative obliteration of different natural builds and the precipitation of different buildup items framed from a complicated series of responses [22]. Table 3 describes the decomposition steps of organo-montmorillonite.

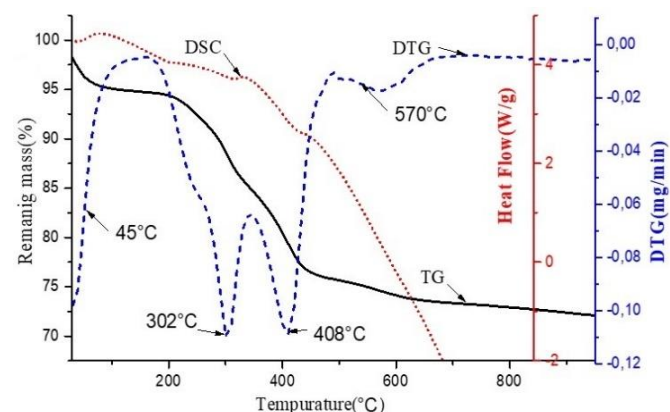


**Figure 6.** TG, DTG and DSC bends of THDACI-MMT

**Table 3.** Decomposition steps of organo-montmorillonites

	FMMT-Na	THDACI-MMT
T <sub>VAP</sub> (H <sub>2</sub> O) °C	52	45
T <sub>DEC</sub> (out) °C	0	302
T <sub>DEC</sub> (in) °C	0	408
T <sub>DEC</sub> (structure) °C	520	570

At 380°C, Figures 7 and 8 show one step in the decomposition of polystyrene. The thermal stability of the nanocomposites was evaluated by thermogravimetric methods. The data listed in Table 4 clearly show that the addition of 1, 3, and 7 weight percent THDACI-MMT to polystyrene improves the thermal stability. Compared to raw polystyrene, the temperature increases by 4°C to 19°C with a 10% reduction in the initial mass of the T<sub>10%</sub> composite. Similarly, the temperature at 50% degradation of the starting mass improves from 8°C to 21°C for T<sub>50%</sub>. The improved thermal behavior of PS/THDACI-MMT nanocomposites over pure PS is due to the formation of carbon (from clay), which acts as a mass transport and insulation between the polymer and the surface area where polymer degradation occurs. This may be due to the formation of carbon (from the clay), which acts as a barrier between mass transport and insulation between the polymer and the surface region where polymer degradation occurs, limiting thermal decomposition of the polymer portion located in the clay gallery.

**Table 4.** The thermal stability of polystyrene and nanocomposites PS/THDACI-MMT (1%, 3%, and 7%) loading

System	PS	PS/THDACI-MMT 1%	PS/THDACI-MMT 3%	PS/THDACI-MMT 7%
T <sub>10%</sub> (°C)	392	396	411	407
T <sub>50%</sub> (°C)	425	433	449	446
T <sub>MAX</sub> (°C)	435	439	454	455
RES (%)	11	9.7	17	13

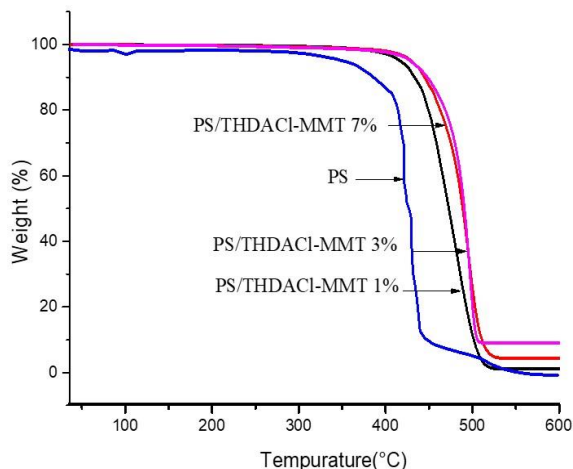


**Figure 7.** TG of PS and PS/ THDACI-MMT (1%, 3%, and 7%) loading

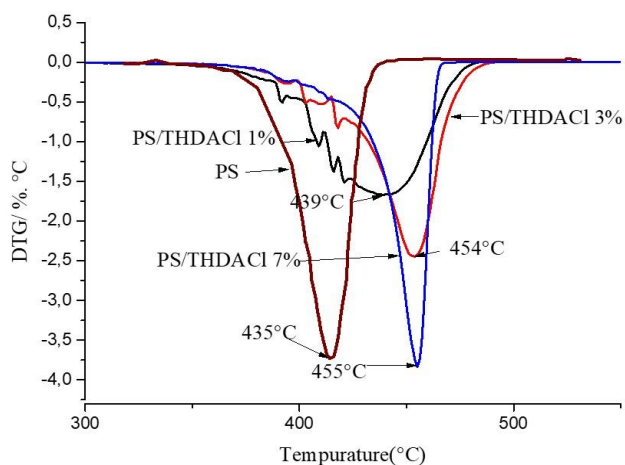


**Figure 8.** DTG of PS and THDACI-MMT (1%, 3%, and 7%) loading

### 3.5 SEM results

For the evaluation of the surface morphology of THDACI-MMT, we relied on SEM analysis. As shown in Figure 9, the surface morphology of the modified MMT exhibits an uneven structure with heterogeneous morphology, as shown in the image; the MMT has a huge and cohesive shape, in some cases with large flakes. The clay surface changed to a non-cohesive

morphology after being altered with polymeric species. This resulted in the formation of large numbers of small flakes with a badly crumpled structure. In addition, the modified MMT surface was also extended because surfactants were present in both materials. In morphogenesis, there are also quite a few microflakes with badly crumpled structures.

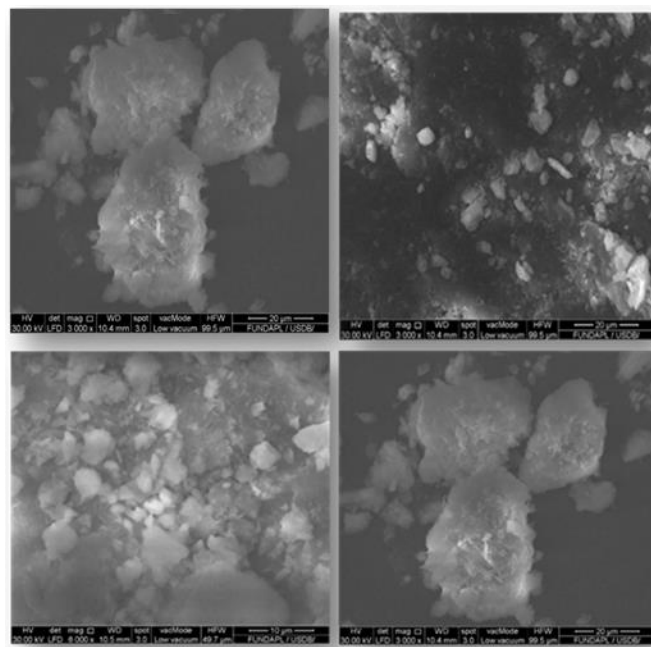


**Figure 9.** SEM images of organoclay THDACI-MMT

### 3.6 TEM results

For the evaluation of the surface morphology of THDACI-MMT, we relied on SEM analysis. As shown in Figure 9, the surface morphology of the modified MMT (Figures 10-11) exhibits an uneven structure with heterogeneous morphology, as shown in the image; the MMT has a huge and cohesive shape, in some cases with large flakes. The clay surface changed to a non-cohesive morphology after being altered with polymeric species. This resulted in the formation of large numbers of small flakes with a badly crumpled structure. In addition, the modified MMT surface was also extended because surfactants were present in both materials. In morphogenesis, there are also quite a few microflakes with badly crumpled structures.

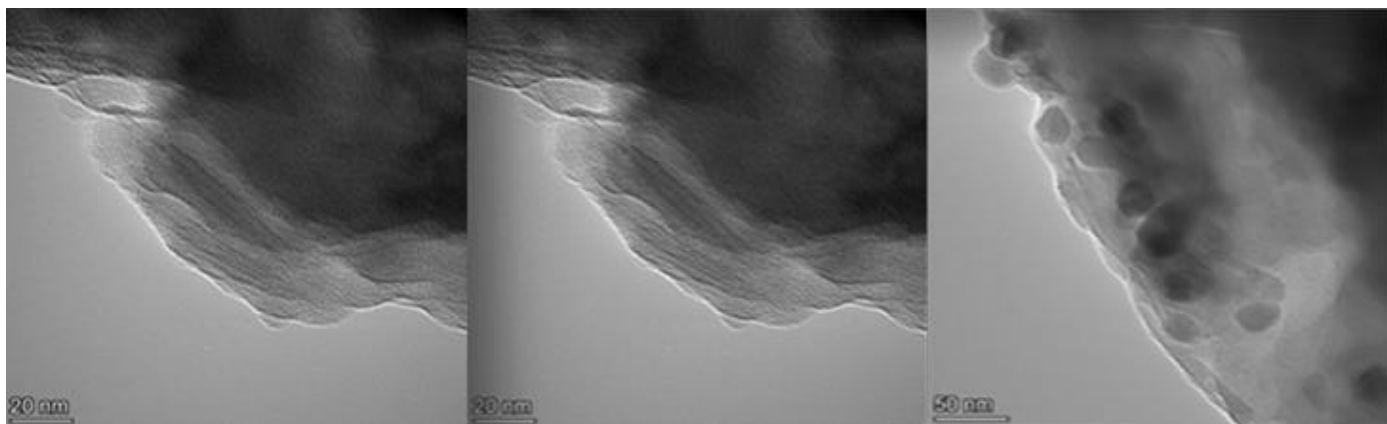


**Figure 10.** TEM micrograph of PS/THDACI-MMT 1% material

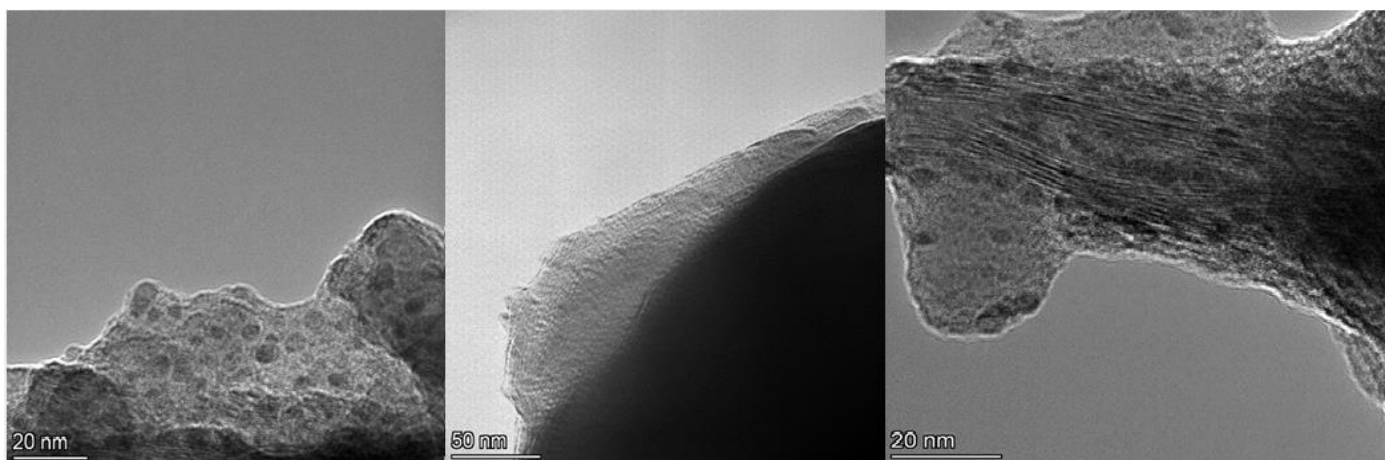


**Figure 11.** TEM micrograph of PS/THDACL-MMT 3% material

#### 4. CONCLUSIONS

In conclusion, this study aimed to investigate the effects of various organo-modifiers on the properties of PS/clay nanocomposites. By systematically studying the dispersion, mechanical properties, thermal stability, and other relevant characteristics of the nanocomposites, we have addressed the research objectives and obtained valuable insights.

The results of this study demonstrate that the choice of organo-modifiers significantly influences the properties of PS/clay nanocomposites. We observed improved dispersion of the nanoclays in the PS matrix, resulting in enhanced mechanical properties, such as increased stiffness and strength. The presence of organo-modifiers also contributed to improved thermal stability, with higher degradation temperatures compared to pure PS. Furthermore, the barrier properties, including gas permeability and water vapor transmission rate, were improved with the incorporation of specific organo-modifiers.

Overall, this study has achieved its research objectives and provided valuable answers and insights into the effects of various organo-modifiers on the properties of PS/clay nanocomposites. The relevance of the obtained results, in relation to the research questions, underscores the significance of this study in advancing the field of polymer clay nanocomposites and guiding future research endeavors.

#### ACKNOWLEDGMENT

The authors thank the Electrochemistry Laboratory of M'sila University, the organic chemistry pedagogical laboratory of M'sila University, also, to the director of the emerging Materials Research Unit of Setif University, and the Directorate of Scientific Research and Technological Development (DGRSDT, MESRS, Algeria) all for the assistance and support to complete this paper.

#### REFERENCES

- [1] Jiang, J., Dun, C., Huang, T., Lu, Z. (2018). Graph convolutional reinforcement learning. arXiv preprint arXiv:1810.09202. <https://doi.org/10.48550/arXiv.1810.09202>
- [2] Ray, S.S., Okamoto, M. (2003). Polymer/layered silicate nanocomposites: A review from preparation to processing. *Progress in Polymer Science*, 28(11): 1539-1641. <https://doi.org/10.1016/j.progpolymsci.2003.08.002>
- [3] Liu, M., Jia, Z., Jia, D., Zhou, C. (2014). Recent advance in research on halloysite nanotubes-polymer nanocomposite. *Progress in Polymer Science*, 39(8): 1498-1525. <https://doi.org/10.1016/j.progpolymsci.2014.04.004>
- [4] Zhang, W., He, X., Li, C., Zhang, X., Lu, C., Zhang, X., Deng, Y. (2014). High performance poly (vinyl alcohol)/cellulose nanocrystals nanocomposites manufactured by injection molding. *Cellulose*, 21: 485-494. <https://doi.org/10.1007/s10570-013-0141-y>
- [5] Li, Y., Han, D., Hu, G., Sommerfeld, M., Hu, Q. (2010). Inhibition of starch synthesis results in overproduction of lipids in *Chlamydomonas reinhardtii*. *Biotechnology and Bioengineering*, 107(2): 258-268. <https://doi.org/10.1002/bit.22807>
- [6] Rhim, J.W., Ng, P.K. (2007). Natural biopolymer-based nanocomposite films for packaging applications. *Critical Reviews in Food Science and Nutrition*, 47(4): 411-433. <https://doi.org/10.1080/10408390600846366>
- [7] He, H.P., Zhu, J. (2017). Analysis of organoclays and organic adsorption by clay minerals. *Developments in Clay Science*, 8: 310-342. <https://doi.org/10.1016/B978-0-08-100355-8.00010-2>
- [8] Wang, H.W., Chang, K.C., Yeh, J.M., Liou, S.J. (2004). Synthesis and dielectric properties of polystyrene-clay nanocomposite materials. *Journal of Applied Polymer Science*, 91(2): 1368-1373. <https://doi.org/10.1002/app.13360>
- [9] Liao, L., Lv, G., Cai, D., Wu, L. (2016). The sequential intercalation of three types of surfactants into sodium montmorillonite. *Applied Clay Science*, 119: 82-86. <https://doi.org/10.1016/j.clay.2015.08.003>
- [10] Xiao, W., Zhan, M., Li, Z. (2003). Organically modifying and modeling analysis of montmorillonites. *Materials & Design*, 24(6): 455-462. <https://doi.org/10.1016/j.msea.2011.01.071>
- [11] Zhu, Y., Iroh, J.O., Rajagopalan, R., Aykanat, A., Vaia, R. (2022). Optimizing the synthesis and thermal properties of conducting polymer-montmorillonite clay nanocomposites. *Energies*, 15(4): 1291.

- <https://doi.org/10.3390/en15041291>
- [12] Unnikrishnan, L., Mohanty, S., Nayak, S.K., Ali, A. (2011). Preparation and characterization of poly (methyl methacrylate)–clay nanocomposites via melt intercalation: Effect of organoclay on thermal, mechanical and flammability properties. *Materials Science and Engineering: A*, 528(12): 3943-3951. <https://doi.org/10.1016/j.msea.2011.01.071>
- [13] Chanra, J., Budianto, E., Soegijono, B. (2019). Surface modification of montmorillonite by the use of organic cations via conventional ion exchange method. In *IOP Conference Series: Materials Science and Engineering*, 13th Joint Conference on Chemistry, Semarang, Indonesia, 509(1): 012057. IOP Publishing. <https://doi.org/10.1088/1757-899X/509/1/012057>
- [14] Madejová, J., Barlog, M., Jankovič, L., Slaný, M., Pálková, H. (2021). Comparative study of alkylammonium- and alkylphosphonium-based analogues of organo-montmorillonites. *Applied Clay Science*, 200: 105894. <https://doi.org/10.1016/j.clay.2020.105894>
- [15] Cole, K.C. (2008). Use of infrared spectroscopy to characterize clay intercalation and exfoliation in polymer nanocomposites. *Macromolecules*, 41(3): 834-843. <https://doi.org/10.1021/ma0628329>
- [16] Ladjal, N., Zidelkheir, B., Terchi, S. (2018). Influence of octadecylammonium, N,N-dimethylhexadecylammonium, and 1-hexadecyltrimethylammonium chloride upon the fractionated montmorillonite: Thermal stability. *Journal of Thermal Analysis and Calorimetry*, 134(2): 881-888. <https://doi.org/10.1007/s10973-018-7237-4>
- [17] Tomić, Z.P., Kaluđerović, L., Nikolić, N., Marković, S., Makreski, P. (2016). Thermal investigation of acetochlor adsorption on inorganic-and organic-modified montmorillonite. *Journal of Thermal Analysis and Calorimetry*, 123: 2313-2319. <https://doi.org/10.1007/s10973-015-5102-2>
- [18] Shirsath, S.R., Patil, A.P., Bhanvase, B.A., Sonawane, S.H. (2015). Ultrasonically prepared poly (acrylamide)-kaolin composite hydrogel for removal of crystal violet dye from wastewater. *Journal of Environmental Chemical Engineering*, 3(2): 1152-1162. <https://doi.org/10.1016/j.jece.2015.04.016>
- [19] Zidelkheir, B., Abdelgoad, M. (2008). Effect of surfactant agent upon the structure of montmorillonite: X-ray diffraction and thermal analysis. *Journal of Thermal Analysis and Calorimetry*, 94(1): 181-187. <https://doi.org/10.1007/s10973-008-9053-8>
- [20] Xi, Y., Zhou, Q., Frost, R.L., He, H. (2007). Thermal stability of octadecyltrimethylammonium bromide modified montmorillonite organoclay. *Journal of Colloid and Interface Science*, 311(2): 347-353. <https://doi.org/10.1016/j.jcis.2007.03.002>
- [21] He, H., Ding, Z., Zhu, J., Yuan, P., Xi, Y., Yang, D., Frost, R.L. (2005). Thermal characterization of surfactant-modified montmorillonites. *Clays and Clay Minerals*, 53(3): 287-293. <https://doi.org/10.1346/CCMN.2005.0530308>
- [22] Yariv, S., Kahr, G., Rub, A. (1988). Thermal analysis of the adsorption of rhodamine 6G by smectite minerals. *Thermochimica Acta*, 135: 299-306. [https://doi.org/10.1016/0040-6031\(88\)87401-X](https://doi.org/10.1016/0040-6031(88)87401-X)
- [23] Chebbi, R., Fadel, A., Aidi, A. (2021). The elimination by natural Algerian clay of chromium ions from salt water. *Annales de Chimie - Science des Matériaux*, 45(2): 105-112. <https://doi.org/10.18280/acsm.450202>

## NOMENCLATURE

$d_{001}$	Polymère/Organo-montmorillonite
$\lambda$	X-ray wavelength
$\theta$	the measured diffraction angle or Bragg angle (°)

## Subscripts

PS/THDACI-MMT	Polymère/Organo-montmorillonite
$T_{VAP}$	The temperature of free water vaporization contained in this montmorillonite
$T_{DEC(out)}$	The surfactant decomposition temperature out the structure
$T_{DEC(in)}$	The surfactant decomposition temperature in the structure
$T_{DEC(structure)}$	The structure decomposition temperature
$T_{10\%}$	10% mass loss temperature
$T_{50\%}$	50% mass loss temperature
$T_{MAX}$	Maximum mass loss temperature
RES	Remaining mass percentage (%)